APPLICATIONS OF
MODELLING AND SIMULATION
http://arqiipubl.com/ams eISSN 2600-8084 VOL 5, 2021, 156-165

Simulation of Erosion Rate in a Reducer for Liquid-Solid Flow System using Computational Fluid Dynamics (CFD)

M. R. Khirham[1], A. Supee[1,2*], R. Md Kasmani[1,2], N. Mohamed Rashid[1,2], A. Sidek[1], N. B. Haladin[3] and Z. Zakaria[4]

[1]School of Chemical and Energy Engineering, Faculty of Engineering, Universiti Teknologi Malaysia, Malaysia
[2]Energy Management Group, School of Chemical and Energy Engineering, Faculty of Engineering, Universiti Teknologi Malaysia, Malaysia
[3]Language Academy, Universiti Teknologi Malaysia, Malaysia
[4]Faculty of Engineering, Universiti Malaysia Sabah, Malaysia

*Corresponding author: aizuddin@utm.my

Submitted 10 May 2021, Revised 21 June 2021, Accepted 30 June 2021.

Abstract: This research aims to simulate the influences of flow parameters such as particles size, stream velocities, and outlet reducer diameter on the erosion rate for a reducer in light crude oil ($C_{19}H_{30}$)-solid (sand) flow system. A commercially accessible ANSYS Fluent 2020 R1 (Academic Version)-computational fluid dynamics (CFD) was applied to numerically simulate the erosion rate in the reducer. Three separate models were used in the CFD approach called as a continuous flow modelling, Lagrangian particle tracking, and empirical erosion equation. The simulated parameters covered 100 - 500 µm particles size, 3 - 7 m/s stream velocities and 0.0762 - 0.1778 m outlet reducer diameter. It was found that the maximum erosion rate increased with the increasing size of the particles and stream velocities and decreased with the increasing of the outlet reducer diameter. For all the simulated parameters, the location of maximum erosion rate was found to be at the outlet location of the reducer except for the reducer with the diameter larger than 0.1270 m whereby it is located at the inlet location of reducer.

Keywords: Computational fluid dynamics (CFD); Light crude oil ($C_{19}H_{30}$)-solid (sand) flow system; Maximum erosion rate and location; Outlet reducer diameter; Particle size and stream velocities.

1. INTRODUCTION

Erosion of liquid-solid impacts is one of the major issues which impacting the stability of structures in many industries including oil and gas as well as power generation sectors. The presence of solid particles in such systems, which cannot be prevented, is the main cause of piping and equipment erosion failure, particularly downstream complex pipe fitting [1-4]. For instance, the oil and gas extracted from the well are inevitably polluted with solid particles, particularly sand, which is a source of several flow assurance problems. Generally, the extracted raw products (i.e., oil, gas, solid particle, and etc.) are transported via gathering pipelines which connecting the well to processing plant (downstream). Practically, these pipelines size ranges from 0.1016 to 0.3048 m (4 to 12 inch) [5]. This type of flow will cause damage to the pipeline system particularly fittings such as elbows, reducer, tee-junctions and some other fluids handling devices such as boilers, heat exchangers, heaters, pumps, and compressors which located at the processing plant due to the erosion phenomenon. If this erosion is not adequately anticipated, monitored and regulated, it could result in shut down for the entire production process for an extended period of time [6].

The prediction of erosion is usually performed using metal walls removal often caused by solid particles impact to assess the safety of the pipeline system, such as reducer. Throughout the forecast, various factors, such as fluid flow characteristics, particle characteristics, particle impingement details and target surface properties are proven to have a significant impact on erosion phenomenon [7]. Badr et al. [8] studied the effects of flow velocities (1, 5, and 10 m/s) and particles size (10, 100, 200, and 400 µm) on erosion rate of carbon steel reducer with a single diameter ratio of 2:1 (inlet diameter: 200 mm, outlet diameter: 100 mm) for the water-sand flow system. They found that the erosion has been severely attacked at the sudden contraction area and increased in particles size and flow velocities cause in increased in erosion rate. On the other side, the

flow direction (upward/downward) has a significant impact on erosion rate only for the particle size of 400 μm and moderate flow velocity of 5 m/s. Similar results are also obtained by other researchers regarding the location of maximum erosion rate (outlet location of reducer) for X65 carbon steel reducer (inlet diameter is 30 mm and outlet diameter is 18 mm) [2]. In their works, they used experimental and simulation approaches to determine the erosion-corrosion behavior for the water-sand flow system (oilfield formation water-250 to 400 μm sand particles with a load of 1 wt%). With flow velocity of 0.5 m/s, they found that, highest erosion rate occurred at the outlet reducer section (bottom part). The occurrence for maximum erosion rate at the bottom part of reducer is due to significant gravity effects on particle motion which move under low flow velocities condition [8]. In addition, they also conclude that erosion rate increases with the reduction of outlet reducer diameter and the differences in velocity and sand concentration causes the differences in erosion rates at different locations of reducer. For the choke geometry studies (inlet and outlet diameter: 15.875 mm, choke diameter: 6.477 mm) which consist of constriction section similar to the reducer, Darihaki et al. [9] conclude that modifications done to the choke entrance including gradual contraction and initial step entrance as well as rounded corner can reduce the maximum erosion rate significantly for the water-sand (particle diameter: 155 μm) flow system with a velocity of 2.5 m/s. In other works of a water-sand flow system for a pipe protruded in a sudden contraction [10], increased in flow velocities and particles size lead to increased maximum erosion rate. There exists a threshold velocity which is 3 m/s whereby below this value, the erosion rate is insignificant. For the CO_2-sand flow system [11], stokes number obtained due to the particle size variation had resulted in different locations of maximum erosion rate been observed. Low Stokes number produced by 25 μm particle size tends to exhibit maximum erosion rate at the tapered section of gradual contraction geometry meanwhile for the high Stokes number generated by 250 μm particle size, maximum erosion rate occurred at the outlet section of pipe. Other than that, increased in taper angle of gradual contraction geometry from 30° to 75° cause in shifted maximum erosion rate towards contraction section.

Nonetheless, none of the works mentioned above did the simulation in light crude oil ($C_{19}H_{30}$)-solid (sand) flow system. To our knowledge, there is limited research perform in this type of flow system especially involving a reducer. Previously, we studied the erosion phenomenon in light crude oil ($C_{19}H_{30}$)-solid (sand) flow system for the elbows [3] and tee-junctions [4]. In this research, a reducer is selected as the fittings in the piping system for erosion phenomenon investigation mainly due to particles size, stream velocities, and changes in flow cross-sectional area. The prediction of erosion rate in reducer for liquid-solid flow is determined through ANSYS Fluent 2020 R1 (Academic Version)-CFD. CFD generally consists of three models: continuous flow modelling, particles tracking, and erosion rate calculation. A measurement of the flow field is usually solved based on Navier–Stokes equations which mathematically express conservation of momentum and mass for a Newtonian fluid and a set of conditions such as transient or stable state, compressible (varied density) or incompressible (constant density), and laminar (Reynolds number (Re_f) < 2000) or turbulent flows (Reynolds number (Re_f) > 4000). The stable state of a fluid can be defined as the state of flow in which the fluid attributes such as velocity, density, pressure, etc. do not change over time (constant) at any particular moment. While the transient state of flow is defined as the state of flow in which the fluid attributes such as velocity, density, pressure, etc. change with respect to time (varied) at a point in time. Once the flow field is collected, the next step in measuring the erosion is to determine the motion of the particles [12]. The Eulerian or Lagrangian method, based on Newton's second law is commonly used to trace the particles and obtained the impact of parameters [13]. Fundamentally, the Lagrangian method deals with individual particles and calculates the trajectory of each particle separately, whereas the Eulerian method deals with concentration of particles, and calculates the overall diffusion and convection of a number of particles.

In this research, we treat the flow system as a stable state, incompressible, and turbulent as listed in assumptions in Table 1. Furthermore, we opted the Lagrangian method in our particle tracking estimation. Finally, an empirical erosion equation available in CFD software is used to illustrate the severity of the erosion occurred. The influences of flow parameters in this research include the particles size of 100 - 500 μm, the stream velocities of 3 - 7 m/s, and outlet reducer diameter of 0.0762 - 0.1778 m. The outlet reducer diameter was set to those value by considering the requirement of sudden reduction of size (from 0.2 m inlet reducer-represents the gathering pipelines size) when it is connected to the pipeline system in processing plant (pipeline/complex pipe fitting/fluids handling devices).

2. SIMULATION DESCRIPTION

2.1 Simulation Procedure

There are three stages involved in this simulation of erosion rate named as the continuous flow modelling, the particle tracking and the application of empirical erosion equation. To initiate the continuous flow modelling, the computational grid has been generated and followed by specifying the solution options such as the turbulence model, the inlet and boundary conditions and as well as the operating condition. After obtaining the flow solution at the reducer, the particles were introduced into the flow. The trajectories of droplets and solid particles through the flow field was numerically determined by using the Lagrangian particles tracking approach. The external forces that exerted on the particles were considered during the determination of the particles' trajectory. Information such as the particles impingement on the wall of reducer, the mass loss or suitably addressed as erosion rate was determined by empirical erosion equation. Preceding simulation work, the Reynolds number (Re_f) for fluid system (light crude oil: $C_{19}H_{30}$) have been manually calculated using an equation of:

$$Re_f = \frac{\rho_f V_f \phi_{outlet\ reducer}}{\mu_f} \quad (1)$$

The calculated values for Re_f in each simulated cases have prevailed within the turbulence range (Re > 4000). The reason for selecting the outlet reducer diameter in Re_f calculation is to ensure that the flow inside the reducer is still within the

turbulence range even though the outlet reducer diameter is smaller than the inlet reducer diameter (Re_f calculation using the inlet reducer diameter: Re_f for 3 m/s stream velocity = 12000; Re_f for 7 m/s stream velocity = 28000). This confirmed our assumption for turbulence flow inside the reducer and validate the suitability of Renormalization group (RNG) k-epsilon model (turbulence modelling) elected in this CFD simulation. For all the simulated cases, the length for inlet section prior to reducer section is fixed to 2 m (~10 $\phi_{inlet\ reducer}$) while for the length of outlet section after the reducer section, it is fixed to 1.8 m (~10 largest $\phi_{outlet\ reducer}$). This was done to ensure that simulated flow is fully developed, and no backflow occurs. At the inlet boundary, the velocity for the fluid (light crude oil) in horizontal direction (x-axis) was fixed according to simulated flow case and the sand particles were initially released uniformly at the same fluid velocity as those simulated cases. Meanwhile for the outlet boundary, the gauge pressure is set to 0 Pa. The lists of simulated parameters and assumptions involved in CFD prediction modelling as well as the manual calculation of Reynolds number for a fluid system (prior to simulation work) are given in Table 1. The descriptions of the symbols (nomenclature, Greek symbols, subscripts, superscripts) used in this paper are listed in Table 2.

Table 1. Define parameters and assumptions in CFD simulator and manual calculation of Reynolds number for fluid system (prior to simulation work)

<table>
<tr><td>Parameter</td><td>Description</td></tr>
<tr><td>Turbulence modelling</td><td>Renormalization group (RNG) k-epsilon model</td></tr>
<tr><td>Fluid system</td><td>• Light crude oil ($C_{19}H_{30}$)
• Density (960 kg/m^3)
• Viscosity (0.048 kg/m.s)</td></tr>
<tr><td>Reducer system</td><td>• Material (carbon steel)
• Density (7850 kg/m^3)
• Inlet reducer diameter (0.2 m)</td></tr>
<tr><td>Operating temperature</td><td>• Room temperature (25 °C)</td></tr>
<tr><td>Particles system</td><td>• Material (sand)
• Number of particles (10000)
• Shape (spherical)
• Density (2600 kg/m^3)</td></tr>
<tr><td>Assumptions</td><td>• The flows inside the reducer are turbulence flow
• Incompressible and constant properties of the fluid
• Spherical shape of particles in the particle tracking approach
• Interaction between solid particles and the effect of particles motion on the fluid flow are small and can be neglected</td></tr>
<tr><td>Simulated flow case</td><td>
<table>
<tr><th>Case</th><th>Manipulated parameters</th><th>Stream velocity (m/s)</th><th>Outlet reducer diameter (m)</th><th>Size of particles (μm)</th><th>Reynolds number calculation for fluid system</th></tr>
<tr><td>1</td><td>Size of particles (μm):
100
200
300
400
500</td><td>7</td><td>0.0762</td><td>-</td><td>10668</td></tr>
<tr><td>2</td><td>Stream velocities (m/s):
3
4
5
6
7</td><td>-</td><td>0.0762</td><td>500</td><td>4572
6096
7620
9144
10668</td></tr>
<tr><td>3</td><td>Outlet reducer diameter (m):
0.0762
0.1016
0.1270
0.1524
0.1778</td><td>7</td><td>-</td><td>500</td><td>10668
14224
17780
21336
24892</td></tr>
</table>
</td></tr>
</table>

Table 2. Descriptions of the symbols

Nomenclature		**Greek symbols**	
x	space coordinate	ρ	density
$\bar{U}$	time average velocity component	μ	viscosity
P	pressure	δ_{ij}	Kronecker delta
u	fluctuating component of velocity	σ_k	effective Prandtl number for k
k	kinetic energy of turbulence	σ_ε	effective Prandtl number for ε
$C_\mu, C_{\varepsilon 1}, C_{\varepsilon 2}$	empirical constants in k-epsilon turbulence model	ε	rate of dissipation of the kinetic energy
G_k	production of turbulent kinetic energy owing to the mean velocity gradients	ϕ	diameter
F	force	∂	partial derivative
m	mass		
V	velocity	**Subscripts**	
C_D	drag coefficient	i, j	spatial coordinate indices
Re_f	fluid Reynolds number	f	fluid
Re_s	particle relative Reynolds number	T	turbulence
t	time	eff	effective
g	gravity	D	drag
$\dot{m}$	mass flow rate	P	pressure gradient
ER	erosion rate	B	buoyancy
$C(\phi)$	function of the diameter	A	added mass
$f(\alpha)$	function of the impact angle	p	particle
V	relative velocity	$face$	wall face where the particles attacks the boundary
A	area		
t	time		
Superscripts			
___	time average		
.	time rate		
b(V)	function of relative velocity		

2.2 The Continuous Flow Modelling

The equations for mass and momentum conservation in addition to the equations representing the turbulence model were used to simulate the flow pattern of the continuous flow phase and that mentioned equations are explained as followed [14-17]:
Mass conservation equation:

$$\left(\frac{\partial}{\partial x_i}\right)(\rho \bar{U}_i) = 0 \tag{2}$$

Momentum conservation equation:

$$\left(\frac{\partial}{\partial x_j}\right)(\rho \bar{U}_i \bar{U}_j) = -\left(\frac{\partial \bar{P}}{\partial x_i}\right) + \left(\frac{\partial}{\partial x_j}\right)\mu\left(\frac{\partial \bar{U}_i}{\partial x_j}\right) - \left(\frac{\partial}{\partial x_j}\right)(\rho\overline{u_i u_j}) \tag{3}$$

where P in momentum Equation (2) is the static pressure and the stress tensor notation ($\rho\overline{u_i u_j}$) can be linked as follows:

$$-\rho\overline{u_i u_j} = \mu_T\left(\frac{\partial \bar{U}_i}{\partial x_j} + \frac{\partial \bar{U}_j}{\partial x_j}\right) - \frac{2}{3}\rho k \delta_{ij} \tag{4}$$

The $\delta_{ij} = 0$ if $i \neq j$, $\delta_{ij} = 1$ if $i = j$, and effective viscosity, $\mu_{eff} = \mu_T + \mu$ where δ_{ij} is Kronecker delta and turbulence viscosity, μ_T is given by:

$$\mu_T = \rho\, C_\mu \left(\frac{k^2}{\varepsilon}\right) \tag{5}$$

with $C_\mu = 0.0845$. Equation (5) was attained by solving both the turbulence modelling equations (Equation (6) and Equation (7)). The equation for kinetic energy of turbulence can be described as follows:

$$\left(\frac{\partial}{\partial x_j}\right)(\rho \bar{U}_j k) = \left(\frac{\partial}{\partial x_j}\right)\left[\left(\frac{\mu_{eff}}{\sigma_k}\right)\left(\frac{\partial k}{\partial x_i}\right)\right] + G_k - \rho\varepsilon \tag{6}$$

The dissipation rate of kinetic energy in turbulence is given by:

$$\left(\frac{\partial}{\partial x_j}\right)\left(\rho \bar{U}_j \varepsilon\right) = \left(\frac{\partial}{\partial x_i}\right)\left[\left(\frac{\mu_{eff}}{\sigma_\varepsilon}\right)\left(\frac{\partial \varepsilon}{\partial x_i}\right)\right] + C_{\varepsilon 1} G_k \left(\frac{\varepsilon}{k}\right) - (C_{\varepsilon 2} + C_{\varepsilon 3})\rho\left(\frac{\varepsilon^2}{k}\right) \quad (7)$$

where G_k represents the production of turbulent kinetic energy owing to the mean velocity gradients and it is explained as followed:

$$G_k = -\rho\overline{u_i u_j}\left(\frac{\partial \bar{U}_j}{\partial x_i}\right) \quad (8)$$

The σ_k and σ_ε are the effective Prandtl numbers for k and ε respectively and $C_{\varepsilon 3}$ as a function of the k/ε are given by previous researchers [18]. The model values for $C_{\varepsilon 1}$ and $C_{\varepsilon 2}$ are set to 1.42 and 1.68.

2.3 Particle Tracking

Eulerian and Lagrangian approaches are used by previous researchers to numerically determine the trajectories of droplets and solid particles through the flow field [19]. Durst et al. [19] has concluded that the Lagrangian approach has some distinct advantages for predicting the particulate flows which possess a large acceleration. Lagrangian can also handle the particulate two-phase flows consisting of polydispersed particle size distribution. In this research, the Lagrangian particles tracking approach has been elected in determining the velocity of the particles as well as its trajectory before any impact towards a reducer wall. By using the Lagrangian particles tracking approach, solid surface erosion and determination of particle trajectory during the motion of the following impact can be estimated. Based on Newton's second law, governing equations of particles motion have been applied in this research and it is described as [11]:

$$m_p\left(\frac{dV_p}{dt}\right) = F_D + F_P + F_B + F_A \quad (9)$$

Equation (9) comprises of drag force (F_D), pressure gradient force (F_P), buoyancy force (F_B) and added mass force (F_A) with the following formula:

$$F_D = C_D \rho_f \pi \frac{\phi_p^2 |V_f - V_p|(V_f - V_p)}{8} \quad (10)$$

where C_D is the drag coefficient and it is given by:

$$C_D = \left(\frac{24}{Re_s}\right)(1 + 0.15 Re_s^{0.687}) \quad (11)$$

The particle relative Reynold number Re_s and other parameters are defined by:

$$Re_s = \frac{[\rho_f |V_p - V_f| \phi_p]}{\mu_f} \quad (12)$$

$$F_P = \pi \phi_p^3 \nabla \frac{P}{4} \quad (13)$$

$$F_B = \pi \frac{\phi_p^3 (\rho_p - \rho_f) g}{6} \quad (14)$$

$$F_A = -\frac{\pi \phi_p^3 \rho_p dV_p}{12 dt} \quad (15)$$

2.4 Erosion Rate (ER) Calculations

The model accessible in the ANSYS Fluent 2020 R1 (Academic Version)-CFD for the *ER* calculation has been adopted by considering the parameters such as function of particles diameter ($C(\phi_p)$), function of the impact angle ($f(\alpha)$), mass flow rate of the particles ($\dot{m}_p$), relative particles velocity (V_p), the function of relative particles velocity ($b(V_p)$) and the area of the wall face where the particles attack the boundary (A_{face}). The empirical erosion equation used is described as follows:

$$ER = \sum_{i=1}^{Nparticle} \dot{m}_p \frac{C(\phi_p) f(\alpha) V_p^{b(Vp)}}{A_{face}} \quad (16)$$

In *ER* calculation, default values of specified function, $C = 1.8 \times 10^{-9}, f = 1,$ and $b = 0,$ were used, while for the other values of parameters, they are imported and processed directly from particle tracking stage in Section 2.3.

3. RESULTS AND DISCUSSION

Three parameters were changed to elucidates their influences on the erosion rate of the reducer component. Those parameters are the size of particles (100 - 500 µm), stream velocities (3 - 7 m/s) and outlet reducer diameter (0.0762 - 0.1778 m). During simulations, another two parameters were set to constant for each simulated flow cases as mentioned in Table 1. The influences of flow cases for the size of particles, stream velocities and outlet reducer diameter on erosion rate of the reducer component are presented in the form of maximum erosion rate graphs and visual illustration of erosion rate surface contours.

3.1 Influences of Particles Size on Erosion Rate in Reducer (Flow Case 1)

The visual illustration of erosion rate surface contours for reducer under various particles size are shown in Figure 1 to Figure 5. Maximum erosion rate was increased with increased in particles size. The trend obtained exhibit similarity with previous works [8, 10]. As fluid flows through the reducer, the momentum of sand particles is directly proportional to their particles size in which causing the energy and frequency of particles attack the wall surface of reducer increases [2]. The number of particles attacks the unit wall increases due to high particle concentration. With the sufficiently high velocity of 7 m/s and after multiple attacks at a tapered location of reducer, all those particles tend to erode severely at the outlet location of the reducer and these deviated particles finally follow the streamline again. The trajectories for particles size of 100 - 500 µm in our research resemble previous research [11] when they simulated the trajectories of 250 µm particle whereby the maximum erosion rate occurred near to the upper location of outlet reducer diameter. Exceeding the maximum erosion rate location, there is more time for drag force to take those particles further towards downstream. This probably the reason for no erosion contours observed beyond that location.

Table 3 illustrates the maximum erosion rate occurred for the flow case 1. The maximum erosion rate was affected by the size of particles and increased in particles size cause increased in maximum erosion rate. The particle size of 500 µm results in the highest maximum erosion rate which is 4.12 x 10^{-6} kg/m^2.s. Larger particles size lead to higher momentum energy and therefore, produced larger or deeper indentations on the wall of reducer. The larger or the deeper the indentation, the greater the amount of material removed or in other word, the higher the maximum erosion rate. For this research, the size of particles was limited to the range of 100 to 500 µm since this is a common size found in the oil and gas industry [20]. Since the particles size of 500 µm and fixed outlet reducer diameter of 0.0762 m resulted in highest maximum erosion rate for a reducer, they were selected as the fixed variable in order to predict the influences of various stream velocities towards erosion rate in reducer (flow case 2).

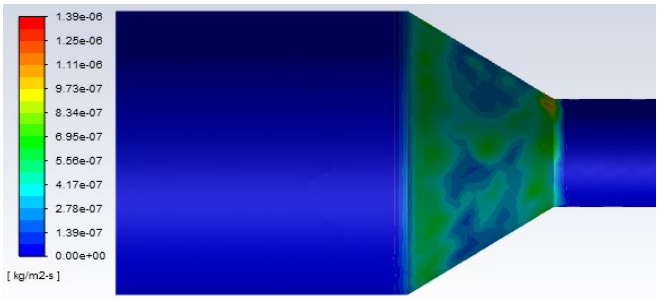

Figure 1. Erosion rate surface contour (kg/m^2.s) for 100 µm particles size

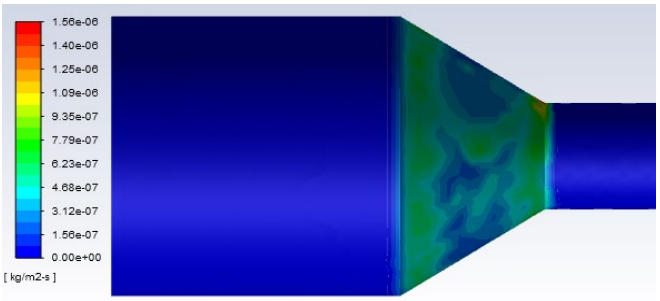

Figure 2. Erosion rate surface contour (kg/m^2.s) for 200 µm particles size

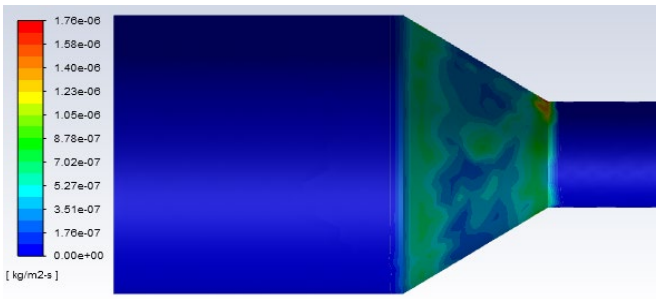

Figure 3. Erosion rate surface contour (kg/m^2.s) for 300 µm particles size

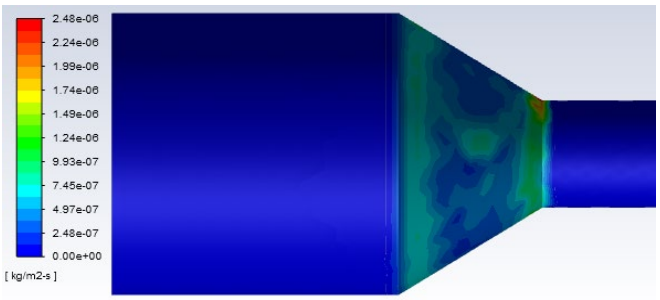

Figure 4. Erosion rate surface contour (kg/m^2.s) for 400 µm particles size

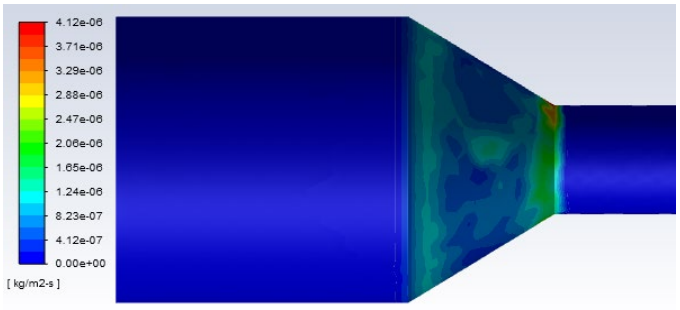

Figure 5. Erosion rate surface contour (kg/m^2.s) for 500 µm particles size

Table 3. Maximum erosion rate (kg/m^2.s) for various particles size (µm)

Particles size (µm)	Maximum erosion rate (kg/m^2.s)
100	1.39 x 10^{-6}
200	1.56 x 10^{-6}
300	1.76 x 10^{-6}
400	2.48 x 10^{-6}
500	4.12 x 10^{-6}

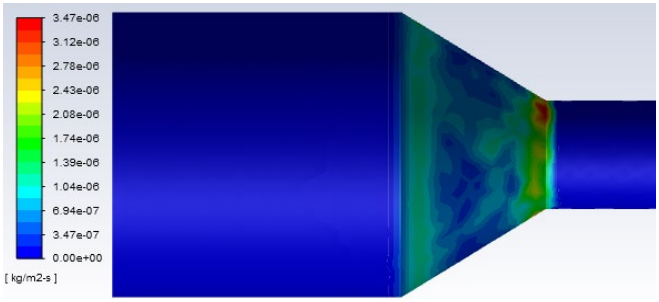

Figure 6. Erosion rate surface contour (kg/m^2.s) for 3 m/s stream velocity

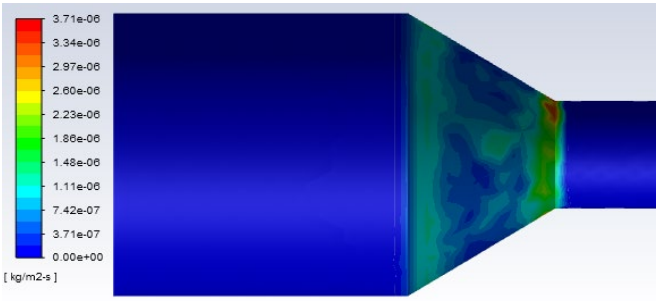

Figure 7. Erosion rate surface contour (kg/m^2.s) for 4 m/s stream velocit

3.2 Influences of Stream Velocities on Erosion Rate in Reducer (Flow Case 2)

Figure 6 to Figure 10 depict the erosion rate surface contours for the simulated reducer at different stream velocities. All the velocities exhibit similarity as flow case 1 in term of the location of the maximum erosion rate whereby it occurred at an upper location of outlet reducer diameter. The likeness may be due to a similar trajectory passed by the particles. Further illustration of the severity values of the erosion rate due to the stream velocities is listed in Table 4. Maximum erosion rate was increased from 3.47 x 10^{-6} kg/m^2.s to 4.12 x 10^{-6} kg/m^2.s when the stream velocity changed from 3 m/s to 7 m/s. The trend obtained also shows a similar pattern with the results obtained from flow case 1 (Table 3). It is interesting to note that the higher the particles size and stream velocity, the greater the maximum erosion rate towards reducer. This due to a larger magnitude of particles momentum caused by higher kinetic energy as the velocity of fluid increases. Based on flow case 1 and flow case 2, the influences of outlet reducer diameter towards erosion rate were determined using the fixed variables which caused the maximum erosion rate which name as the particle size of 500 µm and stream velocity of 7 m/s.

Table 4. Maximum erosion rate (kg/m^2.s) for various stream velocity (m/s)

Stream velocity (m/s)	Maximum erosion rate (kg/m^2.s)
3	3.47 x 10^{-6}
4	3.71 x 10^{-6}
5	3.76 x 10^{-6}
6	3.95 x 10^{-6}
7	4.12 x 10^{-6}

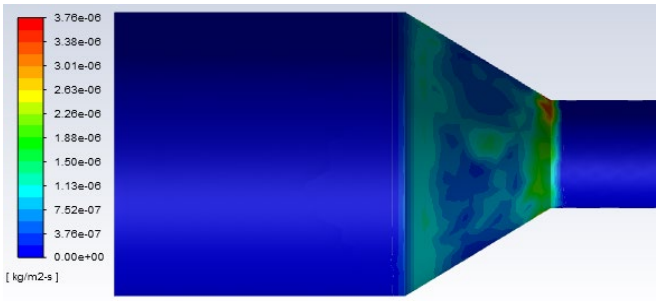

Figure 8. Erosion rate surface contour (kg/m^2.s) for 5 m/s stream velocity

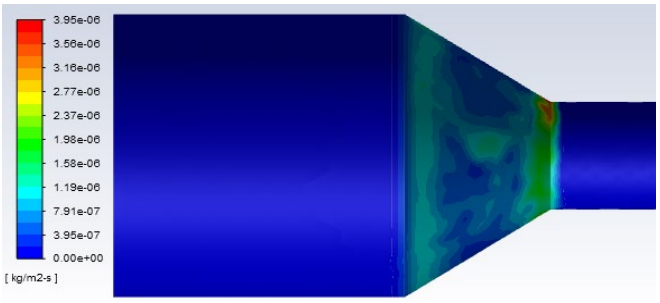

Figure 9. Erosion rate surface contour (kg/m^2.s) for 6 m/s stream velocity

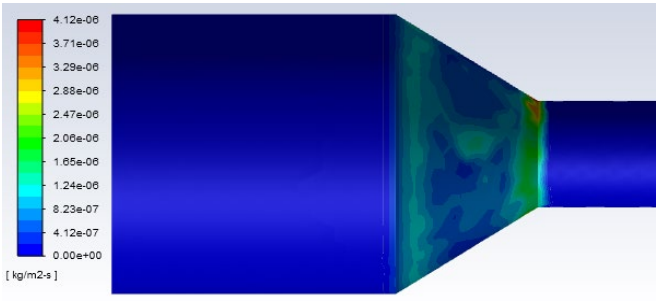

Figure 10. Erosion rate surface contour (kg/m^2.s) for 7 m/s stream velocity

3.3 Influences of Outlet Reducer Diameter on Erosion Rate in Reducer (Flow Case 3)

Erosion rate surface contours for five different size of outlet reducer diameter are shown in Figure 11 to Figure 15. The maximum erosion rate in reducer is to be found at the outlet reducer diameter with shifted from the upper to lower position, for the outlet reducer diameter less than 0.1524 m (Figure 11 to Figure 13). The result in Figure 13 (0.1270 m outlet reducer diameter) shows similarity with previous works whereby the location of maximum erosion rate appeared near to the bottom part of outlet reducer diameter [2], however, the velocity (7 m/s) considered is higher as compared to previous work (0.5 m/s). Thus, it can be concluded that gravity effects for the low flow velocity is not the main causes [8] since the velocity is 14 times larger. Furthermore, for the outlet reducer diameter ≥ 0.1524 m (Figure 14 and Figure 15), the maximum erosion rate occurred at the taper section near to inlet reducer diameter. The reason for this phenomenon to occur is not yet fully understood. However, Liu et al. [2] stated that the differences in stream velocity and sand concentration may cause the differences in erosion rates at different locations for the reducer. Theoretically, changes in the value of outlet reducer diameter will cause changing in stream velocity. This might be the reason for the differences in maximum erosion rate location as shown in Figure 11 to Figure 15. The value of maximum erosion rate for various outlet reducer diameter is listed in Table 5. Smaller outlet reducer diameter will cause in higher maximum erosion rate and vice versa when bigger outlet reducer diameter used. Outlet reducer diameter of 0.0762 m results in the highest maximum erosion rate which is 4.12 x 10^{-6} kg/m^2.s.

Table 5. Maximum erosion rate (kg/m^2.s) for various outlet reducer diameter (m)

Outlet reducer diameter (m)	Maximum erosion rate (kg/m^2.s)
0.0762	4.12 x 10^{-6}
0.1016	1.53 x 10^{-6}
0.1270	9.08 x 10^{-7}
0.1524	5.39 x 10^{-7}
0.1778	5.26 x 10^{-7}

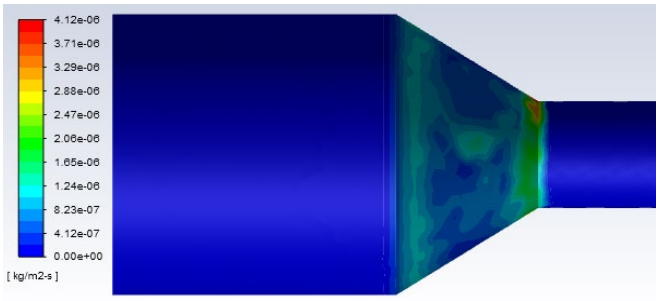

Figure 11. Erosion rate surface contour (kg/m^2.s) for 0.0762 m outlet reducer diameter

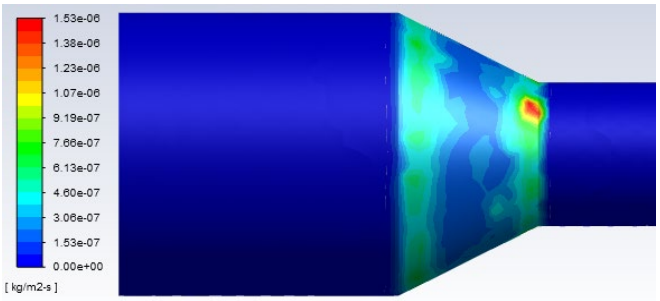

Figure 12. Erosion rate surface contour (kg/m^2.s) for 0.1016 m outlet reducer diameter

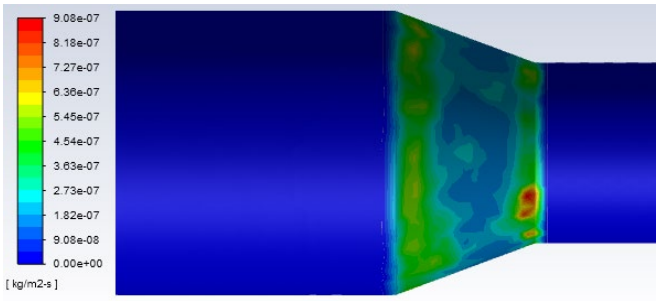

Figure 13. Erosion rate surface contour (kg/m^2.s) for 0.1270 m outlet reducer diameter

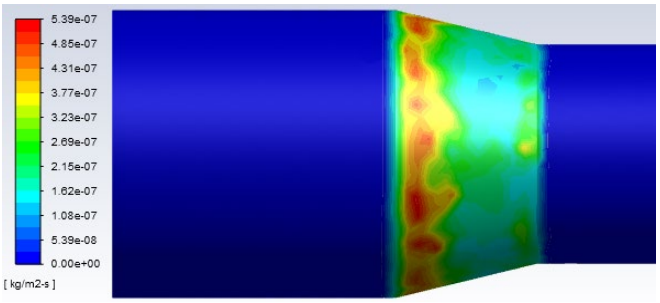

Figure 14. Erosion rate surface contour (kg/m^2.s) for 0.1524 m outlet reducer diameter

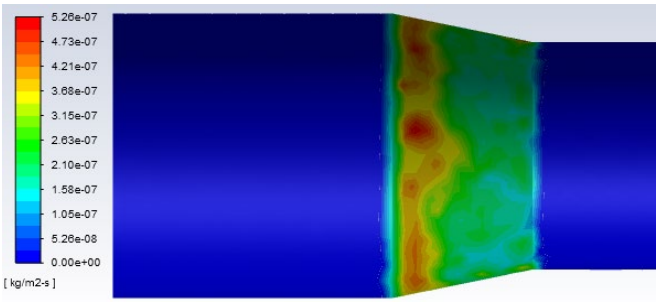

Figure 15. Erosion rate surface contour (kg/m^2.s) for 0.1778 m outlet reducer diameter

4. CONCLUSION

The reducer in light crude oil ($C_{19}H_{30}$)-solid (sand) flow system was simulated under three different flow cases named as the particles size, stream velocities, and outlet reducer diameter using the ANSYS Fluent 2020 R1 (Academic Version)- CFD. Based on the simulation results, it can be deduced that the maximum erosion rate in the reducer is influenced by particles size, stream velocities and outlet reducer diameter. The maximum erosion rate was found to be almost doubled when the size of particles is changed from 100 µm to 500 µm. On the other side, the changes of stream velocities from 3 m/s to 7 m/s cause in slight increased (about 19% increment) in maximum erosion rate. Meanwhile, for the outlet reducer diameter, the maximum erosion rate was decreased to approximately 87% with the increased in outlet reducer diameter from 0.0762 m to 0.1778 m. These simulation results could possibly be used as aided tools in design processes for the field scale applications which possess similar condition and parameters. With an appropriate design, the erosion rate in reducer could be minimized and thus, lessen the maintenance cost in terms of reducer replacement.

ACKNOWLEDGMENT

The authors are grateful to the UTM for interest and encouragement.

REFERENCES

[1] A. Araoye, H. M. Badr, W. H. Ahmed, M. A. Habib and A. Alsarkhi, Erosion of a multistage orifice due to liquid-solid flow, *Wear*, 390-391, 2017, 270-282.

[2] J. Liu, J. Wang and W. Hu, Erosion–corrosion behavior of X65 carbon steel in oilfield formation water, *International Journal of Electrochemical Science*, 14, 2019, 262-278.
[3] M. A. H. Yusof, Z. Zakaria, A. Supee and M. Z. M. Yusop, Prediction of erosion rate in elbows for liquid-solid flow via computational fluid dynamics (CFD), *Applications of Modelling and Simulation*, 3(1), 2019, 28-38.
[4] Z. A. Abang Jashmady, A. Supee, M. D. M. Samsudin and N. B. Haladin, Forecasting of erosion rate in tee-junctions for liquid-solid flow via computational fluid dynamics (CFD), *Applications of Modelling and Simulation*, 4, 2020, 280-289.
[5] Canada's Oil & Natural Gas Producers, *Best management practice: Mitigation of external corrosion on buried carbon steel pipeline*, 2018.
[6] A. Abdulla, *Estimating erosion in oil and gas pipe line due to sand presence*, M.Sc. Thesis, Blekinge Institute of Technology, Karlshamn, Sweden, 2011.
[7] M. Parsi, K. Najmi, F. Najafifard, S. Hassani, B. S. McLaury and S. A. Shirazi, A comprehensive review of solid particle erosion modeling for oil and gas wells and pipelines applications, *Journal of Natural Gas Science and Engineering*, 21, 2014, 850-873.
[8] H. M. Badr, M. A. Habib, R. Ben-Mansour and S. A. M. Said, Effect of flow velocity and particle size on erosion in a pipe with sudden contraction, *Proceedings of the 6th Saudi Engineering Conference*, Dhahran, Saudi Arabia, 2002, pp. 79-88.
[9] F. Darihaki, E. Hajidavalloo, A. Ghasemzadeh and G. A. Safian, Erosion prediction for slurry flow in choke geometry, *Wear*, 372, 2017, 42-53.
[10] M. A. Habib, R. Ben-Mansour, H. M. Badr and M. E. Kabir, Erosion and penetration rates of a pipe protruded in a sudden contraction, *Computers and Fluids*, 37(2), 2008, 146-160.
[11] F. Darihaki, J. Zhang and S. A. Shirazi, Solid particle erosion in gradual contraction geometry for a gas-solid system, *Wear*, 426, 2019, 643-651.
[12] R. J. K. Wood, T. F. Jones, J. Ganeshalingam and N. J. Miles, Comparison of predicted and experimental erosion estimates in slurry ducts, *Wear*, 256(9-10), 2004, 937-947.
[13] H. Zhu, Q. Han, J. Wang, S. He and D. Wang, Numerical investigation of the process and flow erosion of flushing oil tank with nitrogen, *Powder Technology*, 275, 2015, 12-24.
[14] M. A. Habib, H. M. Badr, R. Ben-Mansour and M. E. Kabir, Erosion rate correlations of a pipe protruded in an abrupt pipe contraction, *International Journal of Impact Engineering*, 34(8), 2007, 1350-1369.
[15] M. Cable, *An evaluation of turbulence models for the numerical study of forced and natural convective flow in Atria*, M.Sc. Thesis, Queen's University, Ontario, Canada, 2009.
[16] N. H. Saeid, Numerical predictions of sand erosion in a choke valve, *Journal of Mechanical Engineering and Sciences*, 12(4), 2018, 3988-4000.
[17] N. H. Saeid and R. Rosli, Numerical prediction of sand erosion in elbows, *IOP Conference Series: Materials Science and Engineering*, 686, 2019, 012001.
[18] T. -H. Shih, W. W. Liou, A. Shabbir, Z. Yang and J. Zhu, A new k-ϵ eddy viscosity model for high Reynolds number turbulent flows, *Computers and Fluids*, 24(3), 1995, 227-238.
[19] F. Durst, D. Miloievic and B. Schönung, Eulerian and Lagrangian predictions of particulate two-phase flows: A numerical study, A*pplied Mathematical Modelling*, 8(2), 1984, 101-115.
[20] N. Barton, Erosion in elbows in hydrocarbon production systems: Review document, *Research Report*, TÜV NEL Limited*,*115, 2003.